IEEE Photonics Journal
An IEEE Photonics Society Publication

Tunable Multimode Fiber Based Filter and Its Application in Cost-Effective Interrogation of Fiber-Optic Temperature Sensors

Volume 9, Number 2, April 2017

Li Wei
Anum Khattak
Connor Martz
Da-Peng Zhou

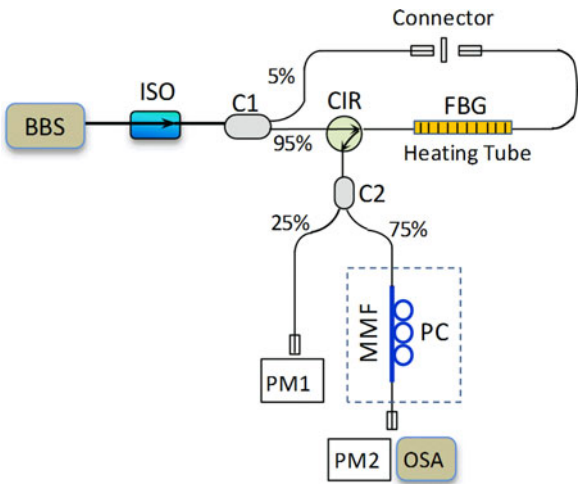

DOI: 10.1109/JPHOT.2017.2679601
1943-0655 © 2017 IEEE

Tunable Multimode Fiber Based Filter and Its Application in Cost-Effective Interrogation of Fiber-Optic Temperature Sensors

Li Wei,[1,2*] Anum Khattak,[1] Connor Martz,[1] and Da-Peng Zhou[3]

[1]Department of Physics and Computer Science, Wilfrid Laurier University, Waterloo, ON N2L 3C5, Canada
[2]Department of Physics and Astronomy, University of Waterloo, ON N2L 3C5, Canada
[3]NFX Systems, Ottawa, ON K1N 6N5, Canada

DOI:10.1109/JPHOT.2017.2679601

Manuscript received December 6, 2016; revised February 27, 2017; accepted March 6, 2017. Date of publication March 9, 2017; date of current version March 27, 2017. This work was supported by the Natural Sciences and Engineering Research Council of Canada (NSERC). Corresponding author: L. Wei (e-mail: lwei@wlu.ca).

Abstract: We present a new tunable all-fiber compact multimode fiber (MMF)-based filter and its applications in fiber sensors. Using the matrix optics approach, we theoretically analyze the transmission characteristics of the tunable filter. The expression of the transmission of the optical filter is the same as that of a regular Mach–Zehnder interferometer (MZI) but with an additional optical phase shift in the sinusoidal function, which makes the MMF-based filter tunable. The phase shift could be changed by properly adjusting a polarization controller where the MMF is simply coiled into. The theoretical result has been verified by our experiment. The proposed tunable filter has been employed for intensity interrogation of a fiber Bragg grating (FBG)-based temperature sensor where the MMF-based filter serves as an edge filter. With the tuning technique, we are able to set the FBG peak to the linear regime of the interference pattern to achieve optimum sensing operation range. By monitoring the optical power changes, it is feasible to obtain information that permits temperature measurement with a simple and low-cost structure.

Index Terms: Tunable optical filters, optical fiber sensors, multimode fibers (MMFs), fiber Bragg grating (FBG).

1. Introduction

The fiber optic sensor has been one of the most important fiber optic devices in numerous industrial applications, for example, in civil engineering, the gas and oil industry, and aerospace, due to their unique advantages of light weight, high sensitivity, long lifetime, and immunity to electro-magnetic interference. The fiber Bragg grating (FBG) has been a popular sensing element by monitoring wavelength shift of the grating to the temperature variation. However, it has a relatively low sensitivity of about 10 pm/°C. To improve the sensitivity, tremendous efforts have been dedicated to different types of interferometers based on the wavelength shift of their interference spectra to the temperature change, for example, the Fabry-Perot interferometer [1], the high-birefringence fiber (HBF) Sagnac interferometer [2], and the Mach-Zehnder interferometer (MZI) [3]–[7]. Among them,

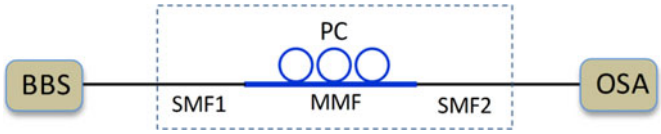

Fig. 1. Experimental setup of all-fiber MZI. SMF1 and SMF2: single mode fiber; MMF: multimode fiber; PC: polarization controller; BBS: broadband source; OSA: optical spectrum analyzer.

MZI has attracted considerable interests due to its simple structure and high sensitivity. Different approaches have been proposed for sensing temperature based on the interference between different modes by employing liquid-core [3], microcavity [4], photonic-crystal fiber (PCF) [5], gourd-shaped microfiber [6], and five-core fiber [7].

On the other hand, studies on fiber-optic sensors reported so far [1]–[7] have mainly focused on wavelength-based monitoring method by using optical spectrum analyzers (OSAs). However, it is very costly, bulky and has slow scanning speed, consequently, increases the complexity of the sensor systems and limits their practical applications. Considerable attention has been paid to develop cost-effective fiber-optic temperature sensors. Passive interrogation methods [8]–[12] have been proposed by using a FBG sensor head along with different types of wavelength-dependent filters to transform the change from the wavelength information into the variation of intensity, for example, cascaded polarization-maintaining fiber (PMF) Sagnac loop filter [8], erbium-doped edge filter [9] and long period grating (LPG) [10]–[12]. Note that LPG is cross sensitive to surrounding medium and fiber bending. Multimode fiber (MMF) based MZI has been proposed by our group for simultaneous measurement of temperature and strain [13]. The applications of MMF-based modal interferometers in fiber sensors [14]–[17] recently have attracted much interest due to their unique features of simple, compact, low cost and easy fabrication. For the use of MMF-based filter as an edge filter for the interrogation of FBG fiber sensors, it is very important to be able to tune the filter such that the center of the FBG locates within the usable linear spectral range. However, little work has been done to address this issue so far.

In this paper, we present a new simple and compact tunable MMF-based filter and its application in cost-effective interrogation of fiber sensors based on a FBG. The MMF used is low-cost commercially available fiber. The proposed MMF filter is a typical modal interferometer constructed with single-mode fiber (SMF) and MMF. To achieve the tunable feature, we coil the MMF into a commercially available 3-paddle polarization controller (PC), and by adjusting the PC, the MMF-based filter can be tuned within a free spectral range. The principle of the tunability will be explained theoretically. With such a filter as an edge filter and a FBG as a sensor element, we are able to monitor the temperature changes in the FBG by measuring the power ratio change after the edge filter without the need of the costly OSA. Furthermore, by varying the length of the MMF, an improved temperature operating range can be achieved.

2. The MMF Based Tunable Filter

Fig. 1 shows the experimental setup of the proposed tunable optical filter. The tunable filter formed by three sections of fibers (SMF-MMF-SMF) being spliced together, serves as a MZI, where the MMF is coiled into a PC in order to enable the filter to be tunable. The SMF-MMF-SMF structure, being intensively studied in the recent years, can naturally create the intermodal interferences. Light starts at the 1st section of SMF1 with only one path (due to single mode nature of the fiber), which is split into multiple paths (because of the excitation of the multiple modes in MMF), and then combined into one path again in the last SMF2 section. Although different paths have the same physical lengths, the difference of the mode effective indices between different modes in MMF gives rise to the interference effect of the MZI. In the proposed configuration, the MMF is coiled into a 3-paddle PC, which will introduce the stress-induced birefringence into the different modes of the MMF. The birefringence intensities of the PC to the fundamental mode and higher order mode are

different. Consequently, an extra phase will be introduced to different paths (i.e., modes), which enables the unique feature of the tunability of the proposed novel all-fiber MZI.

To understand the working principle of the proposed tunable MMF-based filter in Fig. 1, a simple theoretical model is presented, where Jone matrix [18] will be used in the following to construct the mathematical modules. To simplify the theoretical analysis of the tunable property, we assume that only two dominant modes (LP_{01} and LP_{02}) are excited in the MMF [13], [15]; the coupling coefficient of the fundamental mode is κ, and 1-κ for the high-order mode. The attenuation in the fiber is also neglected. By respectively writing the input electric field E^i in SMF1, and E_1 and E_2 at starting point of the MMF for the two dominant modes as $E^i = \left[\begin{smallmatrix} E^{i,x} \\ E^{i,y} \end{smallmatrix}\right]$, $E_1 = \left[\begin{smallmatrix} E_1^x \\ E_1^y \end{smallmatrix}\right] = \sqrt{\kappa}\left[\begin{smallmatrix} E^{i,x} \\ E^{i,y} \end{smallmatrix}\right]$, and $E_2 = \left[\begin{smallmatrix} E_2^x \\ E_2^y \end{smallmatrix}\right] = \sqrt{1-\kappa}\left[\begin{smallmatrix} E^{i,x} \\ E^{i,y} \end{smallmatrix}\right]$, we have the output electric field E_n^o of the two modes at the end of the MMF written as

$$E_n^o = \begin{bmatrix} E_n^{o,x} \\ E_n^{o,y} \end{bmatrix} = e^{j\phi_n} T_n^{PC} \begin{bmatrix} E_n^x \\ E_n^y \end{bmatrix} = e^{j\phi_n} \begin{bmatrix} A_n & B_n \\ C_n & D_n \end{bmatrix} \begin{bmatrix} E_n^x \\ E_n^y \end{bmatrix} \quad (n = 1, 2) \tag{1}$$

with

$$\begin{aligned} &\phi_n = 2\pi n_n L / \lambda \\ &A_n = \cos\delta_n + j \sin\delta_n \cos 2\Omega_n \\ &B_n = C_n = j \sin\delta_n \sin 2\Omega_n \\ &D_n = \cos\delta_n - j \sin\delta_n \cos 2\Omega_n \end{aligned} \quad (n = 1, 2) \tag{2}$$

where $n = 1, 2$ stands for the two different modes; x and y stand for the two orthogonally polarization components; ϕ_n is the linear phase shift of the modes in MMF with a length of L; λ is the operation wavelength and n_n is the effective refractive index of the two modes; T_n^{PC} is the transfer matrix of the PC; Ω_n and δ_n, respectively, stand for the angle of the fast axis orientation of the PC with respect to the x polarization component, and the birefringence intensity attributed to the phase difference between the fast axes and the slow axes of the PC.

By using (1) and (2), we can obtain x and y components of the output electric field of the two modes at the end of the MMF:

$$\begin{aligned} \begin{bmatrix} E_1^{o,x} \\ E_1^{o,y} \end{bmatrix} &= \sqrt{\kappa} e^{j\phi_1} \begin{bmatrix} (\cos\delta_1 + j \sin\delta_1 \cos 2\Omega_1) E^{i,x} + j \sin\delta_1 \sin 2\Omega_1 E^{i,y} \\ j \sin\delta_1 \sin 2\Omega_1 E^{i,x} + (\cos\delta_1 - j \sin\delta_1 \cos 2\Omega_1) E^{i,y} \end{bmatrix} \\ \begin{bmatrix} E_2^{o,x} \\ E_2^{o,y} \end{bmatrix} &= \sqrt{1-\kappa} e^{j\phi_2} \begin{bmatrix} (\cos\delta_2 + j \sin\delta_2 \cos 2\Omega_2) E^{i,x} + j \sin\delta_2 \sin 2\Omega_2 E^{i,y} \\ j \sin\delta_2 \sin 2\Omega_2 E^{i,x} + (\cos\delta_2 - j \sin\delta_2 \cos 2\Omega_2) E^{i,y} \end{bmatrix}. \end{aligned} \tag{3}$$

From (3), one can see that the fundamental mode and the other higher-order mode experience the phase shifts with different amplitudes from fiber itself as well as that from the stress-induced birefringence while propagating along the MMF. When the two modes are combined at the SMF2, from the principle of the superposition the normalized intensity of the resultant wave can be written as

$$T = \frac{\left(E_1^{o,x} + E_2^{o,x}\right)\left(E_1^{o,x} + E_2^{o,x}\right)^* + \left(E_1^{o,y} + E_2^{o,y}\right)\left(E_1^{o,y} + E_2^{o,y}\right)^*}{\left|E^{i,x}\right|^2 + \left|E^{i,y}\right|^2}. \tag{4}$$

By substituting (3) into (4), and having set $E^{i,y} = 0$ for simplification, we can obtain the transmission of the proposed tunable filter

$$T = 1 + 2\sqrt{\kappa(1-\kappa)}\left[M \cos\Delta\phi + N \sin\Delta\phi\right] \tag{5}$$

where

$$\begin{aligned} \Delta\phi &= \phi_1 - \phi_2 = 2\pi(n_1 - n_2)L/\lambda \\ M &= \cos\delta_1 \cos\delta_2 + \sin\delta_1 \sin\delta_2 \cos 2(\Omega_1 - \Omega_2) \\ N &= \cos\delta_1 \sin\delta_2 \cos 2\Omega_2 - \sin\delta_1 \cos\delta_2 \cos 2\Omega_1. \end{aligned} \tag{6}$$

With considering the angle of the fast axis orientations of the PC for the two modes are the same, i.e., $\Omega_1 = \Omega_2$, the coefficients M and N in (6) can be simplified as

$$\begin{aligned} M &= \cos(\delta_1 - \delta_2) \\ N &= -\cos 2\Omega_2 \sin(\delta_1 - \delta_2). \end{aligned} \tag{7}$$

Specifically, when the fast axis orientations of the PC are aligned with x polarization component, i.e., $\Omega_1 = \Omega_2 = 0$, then (5) can be further simplified as

$$T = 1 + 2\sqrt{\kappa(1-\kappa)}\cos(\Delta\phi + \delta_1 - \delta_2). \tag{8}$$

From (8), one can clearly see that the transmission of the proposed filter behaves like the typical two-beam based interferometer, such as traditional MZI, where the contrast of the interference and the free spectral range (FSR) are, respectively, determined by the coupling in the two modes κ and the phase shift $\Delta\phi$ between the fundamental mode and the other high-order mode. From (6), the FSR of the filter can be expressed by

$$FSR = \frac{c}{(n_1 - n_2)L} = \frac{c}{\Delta n \cdot L} \tag{9}$$

where Δn is the modal index difference of the two dominant modes. Note that the significant difference between the conventional MZI and the proposed filter is the presence of the additional phase shift $\delta_1 - \delta_2$ in (8), which is contributed from the difference of the birefringence of the PC induced into the two modes. The additional phase shift could be varied by adjusting the PC. As a result, the proposed MZI filter can be achieved to be tunable. It is worth noting that stress-induced birefringence in MMF in a MZI makes it tunable on wavelength while that in SMF in a fiber loop mirror (FLM) makes it tunable on the reflectivity of the FLM [18].

To verify our theoretical modeling of the proposed tunable filter, experiment has been performed with the setup in Fig. 1. The light from a broadband source (BBS) at L-band is launched to the MMF-based MZI filter (shown in the box in Fig. 1), which is measured by an OSA. The net transmission of the MMF-based MZI filter is obtained by the spectrum of the filter subtracting from the BBS source spectrum to remove the dependence of the spectrum of the BBS. The SMF1 and SMF2 are corning SMF-28 fibers. The MMF fiber is a graded-index multimode fiber which has numerical aperture of 0.29 and core/cladding diameter of 100/140 μm. The PC consists of three small discs with the MMF being coiled, respectively functioning as $\lambda/4$, $\lambda/2$ and $\lambda/4$ wave plates. The transmission spectra of the proposed filter are shown in Fig. 2. The solid line is the spectrum of the filter without adjusting the PC. By suitably adjusting the angular orientations of the three wave plates, consequently varying the birefringence intensity of the two modes, the tunable feature of the MMF-based MZI filter can be achieved as shown in the dotted, dashed, and dash-dotted curves in Fig. 2. The interference fringe pattern is approximately uniform in sinusoidal shape, confirming that two modes primarily interfere while the envelope of the spectrum is slightly modulated by the presence of the higher-order modes. When only considering two dominant modes, the relative power ratio I_2/I_1 in the two modes (LP_{02} and LP_{01}) can be obtained from the extinction ratio (ER) of the tunable filter [19], which is given by

$$I_2/I_1 = \left[\left(1 - 10^{ER/20}\right) \Big/ \left(1 + 10^{ER/20}\right)\right]^2. \tag{10}$$

The ER in (10) is in dB. The ER of the solid line in Fig. 2, converted from the transmission at crest and trough, is about 2.8 dB. The relatively low extinction ratio (about 2.8 dB) of the interference fringe suggests that the power in the LP_{02} mode is relatively as low as 2.6% of the total power. Note

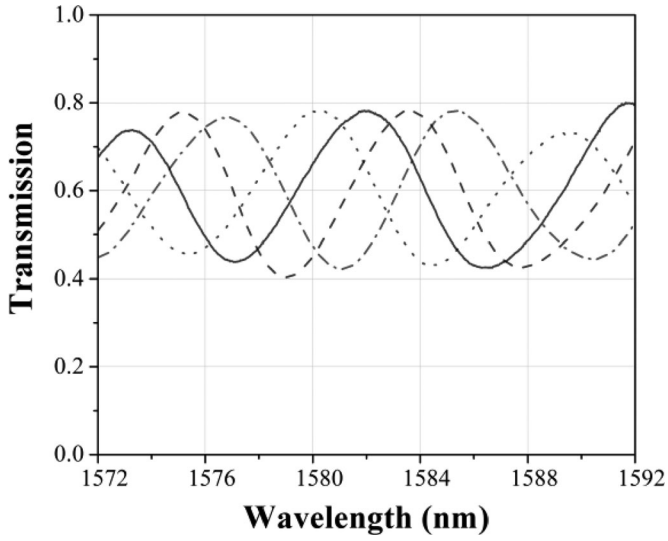

Fig. 2. Transmission spectra of the tunable filter.

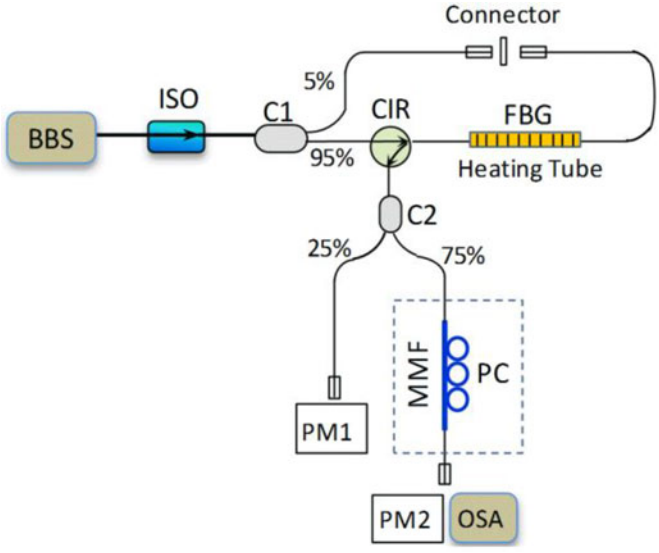

Fig. 3. Experimental setup for the interrogation of temperature sensor with the proposed filter. ISO: isolator; FBG: fiber-Bragg grating; CIR: circulator; C1, C2: couplers; PM1, PM2: power meters.

that the interference depth could be enhanced by splicing the SMF and MMF with a core offset [19]; however, it is accompanied with a large transmission loss.

3. Experimental Results and Discussions

Fig. 3 presents the experimental setup for the interrogation of temperature sensor with the proposed tunable filter. The BBS is used to illuminate an FBG via an optical circulator. The FBG is inserted through a copper tube with a diameter of 1.5 cm, which was wrapped with a heating tape. The FBG was written in standard SMF, with a center wavelength of 1577.462 nm and a bandwidth of 0.2 nm at room temperature. The reflected light from the FBG is split into two paths by a coupler C2 after passing through a circulator. In one path, the intensity P1 is directly measured by a power meter

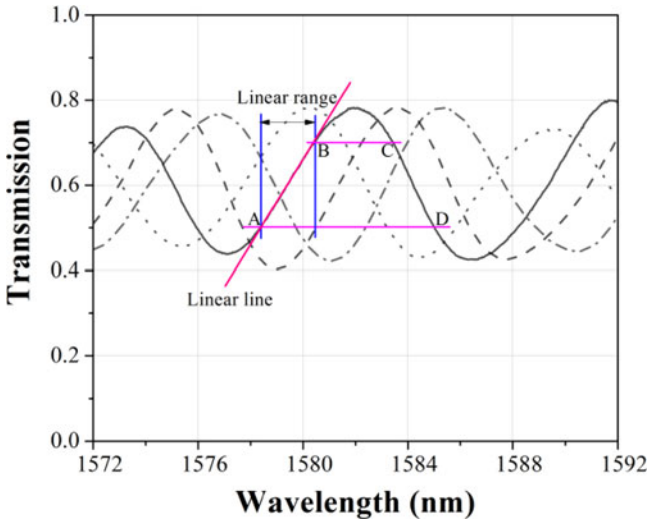

Fig. 4. Useful operating range of the sensor system.

PM1 as a reference to eliminate any power fluctuation and the dependence of the BBS intensity on wavelength; the other path passes through the MMF-based MZI tunable filter (shown in the dashed box) and the intensity P2 is directed measured by another power meter PM2, and the spectrum can be monitored by an OSA.

Here, the MMF-based filter is used as an edge filter which can transform the wavelength shifts to the temperature to intensity variations. The spectrum shape of the interference-based filter is sinusoidal, which means the peak or trough regions cannot be used for this purpose. Only the linear region from A to B, or from C to D, as shown in Fig. 4 can be effectively employed for the intensity interrogation. When the temperature of the FBG increases, the center wavelength of the FBG will have a red wavelength shift. Thus, to ensure having a maximum operating range of the sensor system, the peak of the FBG has to be located in the linear range with starting position at either A or C, which can be implemented by the proposed technique with adjusting the polarization controller to tune the MMF-based filter. This is why it is very important to have the MMF-based filter to be tunable for low-cost interrogation system in the sensing applications in order to achieve the maximum potential. If the testing point starts at Position A (C), we will have a positive (negative) slope of the power vs. wavelength, consequently positive slope of the power vs temperature is expected. The operating range of the sensor system is determined by the wavelength difference ($\lambda_B - \lambda_A$) between position A and B, or wavelength difference ($\lambda_D - \lambda_C$) between position C and D. This indicates that the MMF filter with a larger free spectral range (FSR) will have a wider operating range.

In order to know the exact position of the FBG peak within the MMF interference pattern, we inserted a coupler (C1) with 5% of the coupling ratio and connected the 5% arm to the right side of the FBG, such that the MMF filter can be illuminated by partial of the BBS. Thus, we can monitor the spectrum of the MMF filter along with the FBG at the same frame. In the experiment, we fabricated a 1.5 m long MMF-based filter as shown in Fig. 3. Fig. 5 shows the transmission spectra of the MMF-based filter for different temperatures. As expected, the FBG peak is superimposed on top of the MMF interference pattern; with changing temperature the interference pattern stays still while the peak of the FBG moving accordingly. At room temperature, the starting test point was set at position A (as marked in Fig. 4) by suitably adjusting the PC in order to achieve maximum linearly sensing range with a positive slope. The measured FSR of the filter is about 6 nm, resulting in the effective refractive index difference of 6.24×10^{-4} between the two dominant modes. Note that the small mini peaks on the left side of the FBG is from the FBG itself (as seen in the inset of the

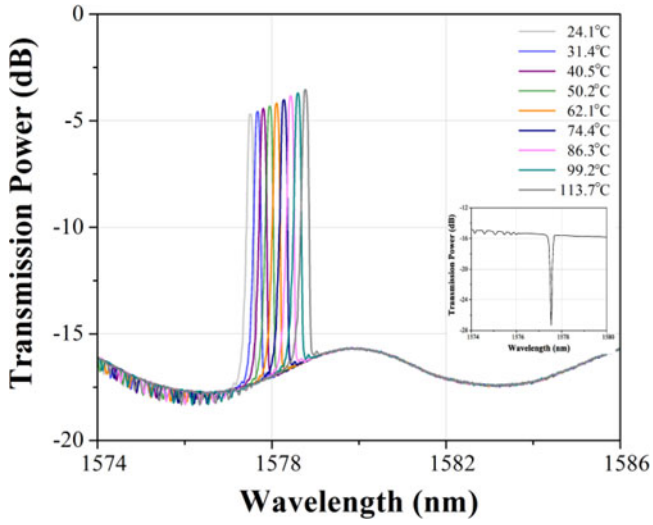

Fig. 5. FBG-superimposed transmission spectra of the MMF-based filter for different temperatures. (Inset) FBG spectrum.

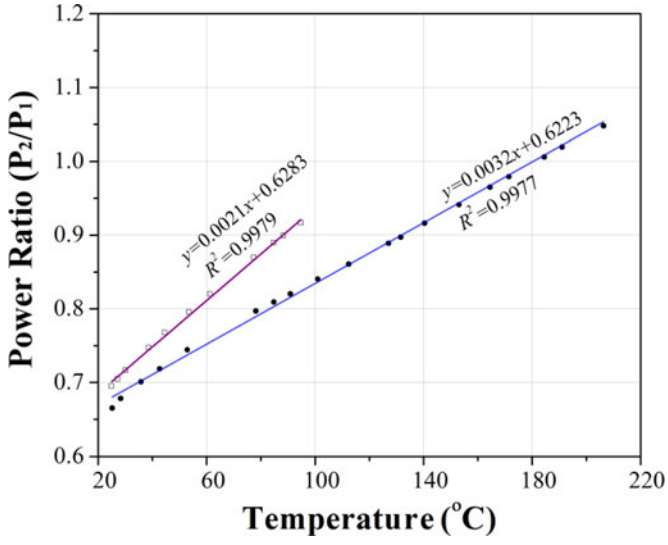

Fig. 6. Power ratio as a function of temperature for different MMF lengths.

figure). When the temperature changes from 24.1 to 113.7 °C, the peak wavelength changes from 1577.495 to 1578.770 nm, corresponding to 14 pm/°C of temperature sensitivity of the FBG.

Once the test starting point is set, we disconnect the connector so the testing results from the power meters (P1 and P2) are all contributed from the reflection signal of the FBG without the background BBS contribution. The power ratio of P_2 to the reference power P_1 is employed to eliminate the BBS wavelength dependence and the source power fluctuation. As mentioned earlier, the operational sensing range of the sensor can be increased by using MMF filter with a large FSR. The FSR of the MMF-based filter is inversely proportional to the length of the MMF from (9). In order to demonstrate how the sensing operation range can be enhanced, we choose two different lengths of the MMF for the experiment. Fig. 6 illustrates the temperature response to the power ratio (P_2/P_1) for 1.5 m long MMF and 1 m long MMF, represented by hollow square and solid circle respectively. The purple and blue lines are the linear-fit lines. It can be seen that there is a good linear relationship between the temperature and the power ratio, and the correlation coefficient

square of R^2 reaches to 0.9979 and 0.9977 for 1.5 m long MMF and 1 m long MMF, respectively. Within the linear region, the temperature range is 70 °C (from 25 °C to 95 °C) for the case of 1.5 m long MMF while the testing temperature range reaches 181 °C (from 25 °C to 216 °C) for the case of 1 m long MMF. As expected, the operational temperature sensing range can be significantly enhanced by choosing the shorter length of MMF.

4. Conclusion

We presented a new tunable all-fiber compact MMF-based filter and its application in fiber sensing. Both theoretical and experimental investigations are performed. Our results show that by suitably adjusting the PC, the filter based on the SMF-MMF-SMF structure can be tuned. This is because the birefringence intensity can be changed by varying the angle of the three plates of the PC, which gives rise to the additional phase shift. This can be used to tune the filter. We demonstrated its application for low-cost interrogation of fiber-optic temperature sensors. With the unique tuning technique, we can shift the FBG peak to the left-side of the linear region of the filter to achieve a maximum sensing operation range for a fixed FSR of the filter. The temperature detection range can be improved by increasing the FSR of the MMF-based filter. The tunable all-fiber MMF-based filter should find useful applications in sensing devices and tunable fiber lasers.

References

[1] D. Jauregui-Vazquez *et al.*, "Modified all-fiber Fabry–Perot interferometer and its refractive index, load, and temperature analyses," *IEEE Photon. J.*, vol. 7, no. 3, Jun. 2015, Art. no. 6600109.

[2] X. Wang, H.-J. Yang, S.-S. Wang, Y.-P. Liao, and J. Wang, "Seawater temperature measurement based on a high-birefringence elliptic fiber Sagnac loop," *IEEE Photon. Tech. Lett.*, vol. 27, no. 16, pp. 1772–1775, Aug. 2015.

[3] M. A. Fuentes-Fuentes, D. A. May-Arrioja, J. R. Guzman-Sepulveda, M. Torres-Cisneros, and J. J. Sánchez-Mondragón, "Highly sensitive liquid core temperature sensor based on multimode interference effects," *Sensors*, vol. 15, pp. 26929–26939, 2015.

[4] L. Jiang, J. Yang, S. Wang, B. Li, and M. Wang, "Fiber Mach–Zehnder interferometer based on microcavities for high-temperature sensing with high sensitivity," *Opt. Lett.*, vol. 36, no. 19, pp. 3753–3755, Oct. 2011.

[5] F. C. Favero, R. Spittel, F. Just, J. Kobelke, M. Rothhardt, and H. Bartelt, "A miniature temperature high germanium doped PCF interferometer sensor," *Opt. Exp.*, vol. 21, no. 25, pp. 30266–30274, 2013.

[6] P. Xian, G. Feng, and S. Zhou, "A compact and stable temperature sensor based on a gourd-shaped microfiber," *IEEE Photon. Tech. Lett.*, vol. 28, no. 1, pp. 95–98, Jan. 2016.

[7] C. Guan, X. Zhong, G. Mao, T. Yuan, J. Yang, and L. Yuan, "In-line Mach-Zehnder interferometric sensor based on a linear five-core fiber," *IEEE Photon. Tech. Lett.*, vol. 27, no. 6, pp. 635–638, Mar. 2015.

[8] C.-S. Kim, T. H. Lee, Y. S. Yu, Y.-G. Han, S. B. Lee, and M. Y. Jeong, "Multi-point interrogation of FBG sensors using cascaded flexible wavelength-division Sagnac loop filters," *Opt. Exp.*, vol. 14, no. 19, pp. 8546–8551, 2006.

[9] U. Tiwari, K. Thyagarajan, M. R. Shenoy, and S. C. Jain, "EDF-based edge-filter interrogation scheme for FBG sensors," *IEEE Sens. J.*, vol. 13, no. 4, pp. 1315–1319, Apr. 2013.

[10] R. W. Fallon, L. Zhang, L. A. Everall, J. A. R. Williams, and I. Bennion, "All-fibre optical sensing system: Bragg grating sensor interrogated by a long-period grating," *Meas. Sci. Technol.*, vol. 9, pp. 1969–1973, 1998.

[11] V. R. Mamidi *et al.*, "Fiber Bragg grating-based high temperature sensor and its low cost interrogation system with enhanced resolution," *Optica Applicata*, vol. 44, no. 2, pp. 299–308, 2014.

[12] V. R. Mamidi, S. Kamineni, L. N. S. P. Ravinuthala, V. Thumu, and V. R. Pachava, "Method to athermalize a long-period fiber grating for interrogation of fiber Bragg grating–based sensors," *Opt. Eng.*, vol. 53, no. 9, pp. 096111–096113, 2014.

[13] D.-P. Zhou, L. Wei, W.-K. Liu, and J. W. Y. Lit, "Simultaneous strain and temperature measurement with fiber Bragg grating and multimode fibers using an intensity-based interrogation method," *IEEE Photon. Tech. Lett.*, vol. 21, no. 7, pp. 468–470, Apr. 2009.

[14] J.-J. Zhu, A. P. Zhang, T.-H. Xia, S. He, and W. Xue, "Fiber-optic high-temperature sensor based on thin-core fiber modal interferometer," *IEEE Sens. J.*, vol. 10, no. 9, pp. 1415–1418, Sep. 2010.

[15] J. Yang *et al.*, "Miniature temperature sensor with Germania-core optical fiber," *Opt. Exp.*, vol. 23, no. 14, pp. 17687–17692, Jun. 2015.

[16] H. Luo *et al.*, "Refractive index sensitivity characteristics near the dispersion turning point of the multimode microfiber-based Mach-Zehnder interferometer," *Opt. Lett.*, vol. 40, no. 21, pp. 5042–5045, 2015.

[17] J. Ruan, P. Huang, Z. Qin, and Q. Zeng, "Temperature characteristic of SMPMS fiber structure-based Sagnac Loop," *IEEE Photon. Tech. Lett.*, vol. 27, no. 1, pp. 62–64, Jan. 2015.

[18] S. Feng, Q. Mao, L. Shang, and J. W. Y. Lit, "Reflectivity characteristics of the fiber loop mirror with a polarization controller," *Opt. Commun.*, vol. 277, no. 2, pp. 322–328, 2007.

[19] B. Dong, D.-P. Zhou, L. Wei, W.-K. Liu, and J. W. Y. Lit, "Temperature- and phase independent lateral force sensor based on a core-offset multi-mode fiber interferometer," *Opt. Exp.*, vol. 16, pp. 19291–19296, 2008.